

Unsupervised Heterophilous Network Embedding via r -Ego Network Discrimination

Zhiqiang Zhong, Guadalupe Gonzalez, Daniele Grattarola, and Jun Pang

Abstract—Recently, supervised network embedding (NE) has emerged as a predominant technique for representing complex systems that take the form of networks, and various downstream node- and network-level tasks have benefited from its remarkable developments. However, unsupervised NE still remains challenging due to the uncertainty in defining a learning objective. In addition, it is still an unexplored research question *whether existing NE methods adapt well to heterophilous networks*. This paper introduces the first empirical study on the influence of homophily ratio on the performance of existing unsupervised NE methods and reveals their limitations. Inspired by our empirical findings, we design unsupervised NE task as an r -ego network discrimination problem and further develop a **SELF-supervised Network Embedding (Selene)** framework for learning useful node representations for both homophilous and heterophilous networks. Specifically, we propose a dual-channel feature embedding mechanism to fuse node attributes and network structure information and leverage a sampling and anonymisation strategy to break the implicit homophily assumption of existing embedding mechanisms. Lastly, we introduce a negative-sample-free SSL objective function to optimise the framework. We conduct extensive experiments and a series of ablation studies on 12 real-world datasets and 20 synthetic networks. Results demonstrate Selene’s superior performance and confirm the effectiveness of each component. Code and data are available at <https://github.com/zhiqiangzhongddu/Selene>.

Index Terms—Heterophilous networks, unsupervised network embedding, self-supervised learning, deep clustering.

I. INTRODUCTION

Following the triumph of machine learning in computer vision and natural language processing, there are more and more success stories coming from machine learning paradigms suited for relational data such as networks or meshes [49]. Network embedding (NE) has become a predominant approach to find effective data representations from complex systems that take the form of networks [8]. Depending on the model’s inherent architecture, existing NE methods can be categorised

into “shallow” or “deep” groups. “Shallow” methods are characterised by an embedding lookup table optimised during training, which directly encodes each vertex as a vector [12], [37], [40], [44]. Despite the relative success of shallow embedding methods, they often ignore node attributes and only focus on the network structural information. This greatly limits their ability to learn expressive representations.

Unlike shallow embedding methods, “deep” methods are often empowered by more complex encoders, usually a deep neural network, enabling the natural modelling of network structures and node attributes [9], [22], [51]. These methods have proven effective in (semi-)supervised settings and have made remarkable breakthroughs in various application areas, such as social networks, e-commerce networks, biology networks, and traffic networks [54]. Nevertheless, the effectiveness of deep methods in unsupervised settings, i.e. how to learn effective representations without any supervision, is relatively unexplored. In addition, recent work demonstrated that classic supervised NE methods have limited representation power on heterophilous networks [4], [25], [56]. For instance, GCN [22] is proven to be a low-frequency filter which will result in indistinguishable node representations on heterophilous networks [4]. And moreover, addressing the heterophily scenario is essential for network analysis and fairness study [19], [26]. In light of these three observations, a natural question arises **RQ1**: *how do existing NE methods perform on heterophilous networks without supervision?*

Contribution. We focus on the effectiveness of NE methods in tackling the node clustering task in a challenging setting: the goal of the task is to group similar nodes into the same category without any manual supervision [15], [34] (for convenience, we will refer to unsupervised network embedding as network embedding in the remainder of the text). Moreover, unlike most prior work which implicitly holds a *homophily* assumption that nodes of the same class tend to be connected, we focus on the more difficult *heterophily* setting where “opposites attract”, i.e., linked nodes are likely to be from different classes.

First, we conduct an empirical study on 20 synthetic networks with a variety of homophily ratios (h) to investigate whether h influences the node clustering performance of representative NE methods (RQ1). Our experimental results, summarised in Figure 2, show that (i) the performance of NE methods that rely on network structure information decreases significantly when $h \rightarrow 0$; (ii) the performance of NE methods that rely on node attributes is not affected by changes of h , and their performance has a significant advantage compared

Zhiqiang Zhong is with the Faculty of Science, Technology and Medicine, University of Luxembourg, Esch-sur-Alzette, Luxembourg.
E-mail: zhiqiang.zhong@uni.lu

Guadalupe Gonzalez is with the Faculty of Engineering, Imperial College London, London, UK.
E-mail: ggg17@ic.ac.uk

Daniele Grattarola is with Faculty of Informatics, Università della Svizzera italiana, Lugano, CH
E-mail: grattdd@usi.ch

Jun Pang is with the Faculty of Science, Technology and Medicine, and the Interdisciplinary Centre for Security, Reliability and Trust, University of Luxembourg, Esch-sur-Alzette, Luxembourg.
E-mail: jun.pang@uni.lu

to other methods when $h < 0.5$. These two findings directly answer RQ1, and meanwhile, raise another interesting and challenging question **RQ2: could we design a NE framework that adapts well to both homophily and heterophily settings?**

Motivated by the limitations mentioned above, we design the NE task as an r -ego network discrimination problem and propose a **SELf-supErvised Network Embedding** (Selene) framework. Conceptually, we propose three solutions to avoid the homophily’s influence on the NE performance and leverage the idea of negative-sample-free self-supervised learning (SSL) to design an optimisation objective for NE. Specifically, we propose a dual-channel features embedding pipeline that integrates node attributes and network structure information. Next, we revisit representative NE mechanisms and propose using r -ego network sampling and anonymisation to break the inherent homophily assumption of NE and introduce network structure features to enhance the framework’s ability to capture structural information. Lastly, we employ a negative-sample-free SSL objective function to optimise the framework.

To summarise, our work makes the following contributions:

- To the best of our knowledge, this is the first work that systematically studies the influence of homophily ratio on unsupervised NE methods’ performance. We reveal the limitations of NE methods to learn over heterophilous networks.
- We present the **SELf-supErvised Network Embedding** (Selene) framework, which adapts well to both homophilous and heterophilous networks.
- Extensive experiments on 12 real-world datasets and 20 synthetic networks demonstrate Selene’s superior performance on challenging node clustering tasks. A series of ablation studies confirm the effectiveness of Selene’s components.

II. ADDITIONAL RELATED WORK

Network embedding before GNNs. NE techniques aim at embedding rich node attributes and structural information in complex systems that take the form of networks into low-dimensional node representations [8]. Depending on the model architecture, NE methods can be naturally categorised into two groups: “shallow” and “deep” methods [10]. Shallow methods comprise an embedding lookup table which directly encode each node as a vector, and is optimised during training. Within this group, several Skip-Gram [31]-based NE methods have been proposed, such as DeepWalk [37] and node2vec [12] as well as their matrix factorisation interpretation NetMF [39], LINE [44] and PTE [43]. DeepWalk generates walk sequences for each node on a network using truncated random walks, and learns node representations by maximising the similarity of representations for nodes that occur in the same walks, thus preserving neighbourhood structures. Node2vec increases the expressivity of DeepWalk by defining a flexible notion of a node’s network neighbourhood and designing a second order random walk strategy to sample the neighbourhood nodes; LINE is a special case of DeepWalk when the size of node’s context is set to one; PTE can be viewed as the joint factorisation of multiple networks’ Laplacians [39]. To better capture the structural identity of nodes independent of network position and neighbourhood’s labels, struc2vec [40]

constructs a hierarchy to encode structural node similarities at different scales. Despite the relative success of shallow embedding methods, they often ignore the richness of node attributes and only focus on the network structural information, which hugely limits their performance.

Network embedding with GNNs. Recently, graph neural networks (GNNs) have shown promising results in modelling structural and relational data [49]. The common idea of capturing nodes’ neighbourhoods to measure nodes’ similarities used by shallow methods can be intuitively generalised with GNN models that follow a recursive neighbourhood aggregation or message-passing scheme. Additionally, GNNs are often powered by more complex encoders, usually a deep neural network, enabling a more expressive modelling of network structure and node attributes. Existing GNN models can be generally categorised into spectral [9], [23], [50] and spatial approaches [13], [22] and can be trained to fit node labels or to reconstruct network structure. Within this field, NE is equivalent to an optimisation problem that encodes network nodes into latent vectors by means of an encoding function, with the objective of ensuring that results decoded from vectors preserve network properties of interest. Several approaches leveraging GNNs, such as ChebNet [9], GCN [22], GraphSAGE [13], CayleyNets [23], GWNN [50] and GIN [51], which fuse node features and neighbourhood structures to compute embeddings, have allowed remarkable breakthroughs in numerous fields under (semi-)supervised settings. However, their effectiveness in NE without manual supervision is relatively unexplored. Recently proposed methods leveraging GNNs with self-supervised learning, such as DGI [47], GMI [36], SDCN [5], and GBT [3] have been introduced for the task of unsupervised NE, primarily being evaluated on homophilous networks.

Heterophilous network embedding. Recent works focused on the NE on heterophilous networks where nodes of different class labels are often connected [4], [7], [25], [56] and have shown that the representation power of GNNs that follow (semi-)supervised settings is greatly limited on heterophilous networks. Nevertheless, how do unsupervised NE methods perform on heterophilous networks is still unexplored.

III. NOTATION AND PRELIMINARIES

An unweighted network with n nodes can be formally represented as $\mathcal{G} = (\mathcal{V}, \mathcal{E}, \mathbf{X})$, where \mathcal{V} is the set of nodes and $|\mathcal{V}| = n$, $\mathcal{E} \subseteq \mathcal{V} \times \mathcal{V}$ denotes the set of edges, and $\mathbf{X} = \{\mathbf{x}_1, \mathbf{x}_2, \dots, \mathbf{x}_n\}$, with each $\mathbf{x}_i \in \mathbb{R}^\pi$, represents node features (π is the dimensionality of node features). And \mathcal{Y} stands for a set with class labels for all $v \in \mathcal{V}$. For subsequent discussion, we summarise \mathcal{V} and \mathcal{E} into an adjacency matrix $\mathbf{A} \in \{0, 1\}^{n \times n}$.

Problem setup. In this paper, we focus on the unsupervised node clustering task on a network \mathcal{G} . We firstly aim to learn precise node representation $\mathbf{H}_v \in \mathbb{R}^d$, with d being the dimensionality of node representations, for all $v \in \mathcal{V}$ by leveraging node attributes and local structure context. Then, we infer the unknown class labels y_v for all $v \in \mathcal{V}$ according to the learned node representation \mathbf{H}_v with a clustering algorithm (we

utilise the well-known algorithm K -means [15] in this paper). Note that, for convenience, we will refer to unsupervised network embedding as network embedding in the subsequent discussion.

Definition 1. (Neighbourhood \mathcal{N}_v). We denote a general neighbourhood around ego node v , excluding v (in case \mathcal{G} has self-loops), as \mathcal{N}_v ; and the corresponding neighbourhood including the ego node v as $\tilde{\mathcal{N}}_v$. The neighbouring nodes of ego node v within r hops are denoted by $\mathcal{N}_v^r = \{v : d(u, v) \leq r\}$, where $d(u, v)$ is the shortest path instance between u and v . For example, for the network shown in Figure 1-(a), $\mathcal{N}_{v_0}^1 = \{v_0, v_1, v_2, v_4, v_7\}$.

Definition 2. (r -ego Network $\mathcal{G}_r(v)$) [30], [38]. For an ego node v of \mathcal{G} , its r -ego neighbours are $\mathcal{N}_v^r \subseteq \mathcal{V}$. The corresponding r -ego network is an induced subnetwork of \mathcal{G} , which is defined as $\mathcal{G}_r(v) = \{\mathcal{N}_v^r, \mathcal{E}_v^r, \mathbf{X}_v^r\}$, where $\mathcal{E}_v^r := ((\mathcal{N}_v^r \times \mathcal{N}_v^r) \cap \mathcal{E})$.

Definition 3. (Homophily Ratio h). For an arbitrary network \mathcal{G} , its homophily ratio h is determined by the relationship between node labels and network structure encoded in the adjacency matrix (\mathbf{A}). Recent work commonly use two *homophily* metrics: edge homophily (h_{edge}) [55] and node homophily (h_{node}) [35]. They can be formulated as:

$$h_{edge} = \frac{|\{(u, v) : (u, v) \in \mathcal{E} \wedge y_u = y_v\}|}{|\mathcal{E}|} \quad (1)$$

$$h_{node} = \frac{1}{|\mathcal{V}|} \sum_{v \in \mathcal{V}} \frac{|\{u : u \in \mathcal{N}_v \wedge y_u = y_v\}|}{|\mathcal{N}_v|}$$

Specifically, h_{edge} evaluates the fraction of edges in a network which connect nodes that have the same class labels; h_{node} evaluates the overall fraction of neighbouring nodes that have the same class labels. In this paper, we focus on edge homophily and set $h = h_{edge}$ in the following sections. Figure 1-(a) demonstrates an example network with $h = 0.2$.

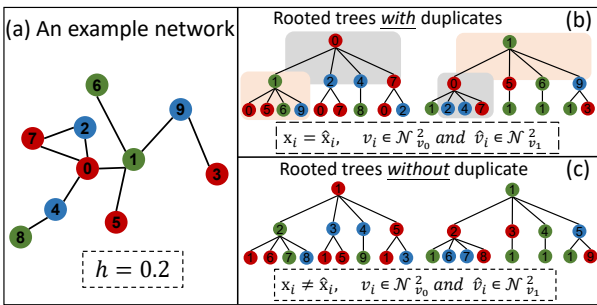


Fig. 1. A toy example of the rooted aggregation trees on an example heterophilous network ($h = 0.2$). Different colours represent different node classes. (a) An example network; (b) Two rooted 2-layers aggregation trees of two connected nodes, i.e., v_0 and v_1 . Duplicated components of two rooted trees are marked with the same shadow colour. (c) After ego network sampling and anonymity, two rooted aggregation trees have no duplicates.

IV. AN EXPERIMENTAL INVESTIGATION

In this section, we empirically analyse the performance of NE methods on 20 synthetic networks with different homophily ratios (h) and node attributes. The main goal is to investigate **(RQ1)**: *how do existing NE methods perform*

on heterophilous networks? Specifically, we quantify their performance on the node clustering task on two sets of synthetic networks, i.e., Synthetic and Synthetic-Products, with $h \in [0, 0.1, \dots, 0.9]$. A detailed description of the synthetic datasets generation process can be found in Section VI-A; and we refer the reader to Section VI-B for details on the experimental settings.

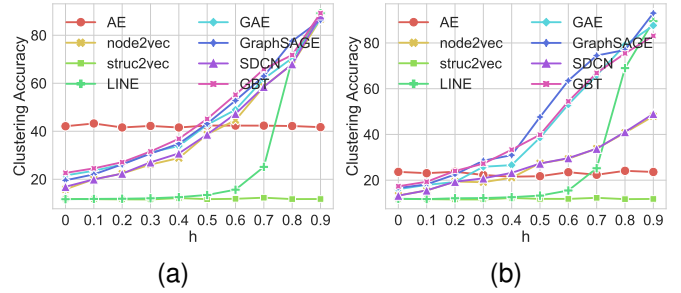


Fig. 2. Node clustering accuracy of representative NE methods on synthetic datasets, i.e., Synthetic (a) and Synthetic-Products (b).

Figure 2 illustrates that with the decrease of h , the clustering accuracy of representative NE methods that rely on network structure, i.e., node2vec [12], LINE [44], GAE [21], GraphSAGE [13], SDCN [5] and GBT [3], decreases significantly. The accuracy of AE [17], which only relies on raw node attributes, remains stable for different values of h and demonstrates apparent advantage on Synthetic (with $h < 0.5$). The reason why existing NE methods using network structure only fail when $h \rightarrow 0$ is that they all implicitly follow a homophily assumption. For instance, objective functions of node2vec, LINE and GraphSAGE, guide nodes at close distance to have similar representations and nodes far away to have different ones. The inherent aggregation mechanism of GAE, GraphSAGE, SDCN and GBT naturally assumes local smoothing [6], [32] (which is mainly caused by the duplicated aggregation tree as shown in Figure 1-(b)), which translates into neighbouring nodes having similar representations. But as shown in Figure 2, NE methods leveraging network structure show outstanding performance with $h \rightarrow 1$. Lastly, it is worth noting that struc2vec [40], which relies on network structure too, performs worse on the 20 synthetic networks. The reason is that struc2vec identifies the structure of ego networks by counting the degree of nodes of different hops. The synthetic network generation process assigns node degree to each node with a normal distribution, i.e., nodes from different classes can have the same degree. Therefore, it is not able to identify the ego network's local structure. This suggests us that neural network-based models have better usability in capturing ego network structure patterns than manual defined statistical methods.

V. PROPOSED APPROACH

In this section, we formalise the main challenges of NE on heterophilous networks. To address these challenges, we present the SELf-supERvised NEtwork Embedding (Selene) framework. Figure 3 shows the overall view of Selene.

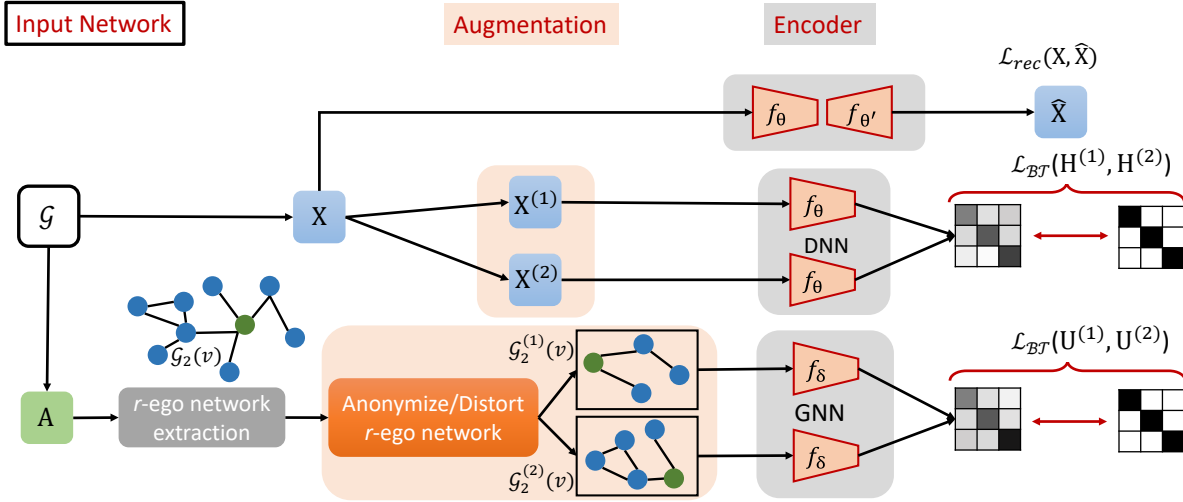


Fig. 3. An illustration of our proposed framework Selene. \mathbf{X} and \mathbf{A} are raw node attributes and adjacency matrix of the input network \mathcal{G} , respectively. $\mathbf{X}^{(1)}$ and $\mathbf{X}^{(2)}$ are two distorted node attribute matrix, $\hat{\mathbf{X}}$ is the reconstructed node attribute matrix. Extracted r -ego network ($\mathcal{G}_r(v)$) of ego node v will be anonymised to break its connection to neighbour nodes, and then distorted to two ego networks, i.e., $\mathcal{G}_2^{(1)}(v)$ and $\mathcal{G}_2^{(2)}(v)$. Node attribute encoder is optimised by the reconstruction loss $\mathcal{L}_{rec}(\mathbf{X}, \hat{\mathbf{X}})$ and attribute Barlow-Twins loss $\mathcal{L}_{BT}(\mathbf{H}^{(1)}, \mathbf{H}^{(2)})$; network structure encoder is optimised by the network Barlow-Twins loss $\mathcal{L}_{BT}(\mathbf{U}^{(1)}, \mathbf{U}^{(2)})$. The final node representation obtained by applying COMBINE to the generated node attribute representation \mathbf{H} and network structure representation \mathbf{U} .

Challenges. As we discussed in Section IV, it is crucial to involve both node attributes and network structure information into the NE model to learn expressive node representations by identifying and distinguishing differences among different nodes. Existing methods address this challenge by reconstructing the network structure [21], node attributes [5], [17] or by assuming that nodes close to each other tend to have similar node representations [12], [13], [37]. However, these solutions are not suitable for heterophilous networks as shown in Section IV. Therefore, the design of an appropriate learning objective is a key challenge to address in this work. In the remainder of this section, we will address the following research challenges:

- RC1** How to leverage node attributes and network structure for network embedding?
- RC2** How to break the inherent homophily assumptions of traditional network embedding mechanisms?
- RC3** How to define an appropriate objective function to optimise the embedding learning process?

A. Dual-channel Feature Embedding (RC1)

The empirical analysis of Section IV highlighted that node attributes play a major role in the performance of NE methods, especially on heterophilous networks. Therefore, we propose a dual-channel feature embedding pipeline to learn node representation from node attributes and network structure separately, as shown in Figure 3. Such a design brings two main benefits: (i) both sources of information can be well utilised without interfering with each other, and (ii) the inherent homophily assumptions of NE methods can be greatly alleviated, an issue we will address in the next subsection.

Node attribute encoder module. As previously mentioned, learning effective node attribute representations is of great importance for NE. There are several alternative methods to

learn representations for different types of data, including Autoencoder [17] and its derived variants [27]–[29]. In this paper, we employ the basic Autoencoder to learn representations of raw node attributes, which can be replaced by more sophisticated encoders to obtain higher performance. We assume an L -layer Autoencoder, with the formulation of the ℓ -th encoding layer being:

$$\mathbf{H}_e^{(\ell)} = \phi(\mathbf{W}_e^{(\ell)} \mathbf{H}_e^{(\ell-1)} + \mathbf{b}_e^{(\ell)}) \quad (2)$$

where ϕ is a non-linear activation function such as ReLU [33] or PReLU [16]. $\mathbf{H}_e^{(\ell-1)} \in \mathbb{R}^{n \times d_{\ell-1}}$ is the hidden node attribute representations in layer $\ell-1$, with $d_{\ell-1}$ being the dimensionality of this layer's hidden representation. $\mathbf{W}_e^{(\ell)} \in \mathbb{R}^{d_{\ell-1} \times d_\ell}$ and $\mathbf{b}_e^{(\ell)} \in \mathbb{R}^{d_\ell}$ are trainable weight matrix and bias of the ℓ -th layer in the encoder. Node representations $\mathbf{H} = \mathbf{H}_e^{(L)}$ are obtained after successive application of L encoding layers.

Following the encoder, the decoder reconstructs input node attributes from the computed node representations \mathbf{H} . Typically, a decoder has the same structure as the encoder by reversing the order of layers. Its ℓ -th fully connected layer can be formally represented:

$$\mathbf{H}_d^{(\ell)} = \phi(\mathbf{W}_d^{(\ell)} \mathbf{H}_d^{(\ell-1)} + \mathbf{b}_d^{(\ell)}) \quad (3)$$

where $\mathbf{W}_d^{(\ell)}$ and $\mathbf{b}_d^{(\ell)}$ are trainable weight matrix and bias of ℓ -th layer in the decoder, respectively. Reconstructed node attributes $\hat{\mathbf{X}} = \mathbf{H}_d^{(L)}$ are obtained after successive applications of L decoding layers. We optimise the autoencoder parameters by minimising the difference between raw node attributes \mathbf{X} and reconstructed node attributes $\hat{\mathbf{X}}$ with:

$$\mathcal{L}_{rec}(\mathbf{X}, \hat{\mathbf{X}}) = \frac{1}{2|\mathcal{V}|} \|\mathbf{X} - \hat{\mathbf{X}}\|_F^2 \quad (4)$$

B. *r*-ego Network Sampling and Anonymity (RC2)

The success of GNN-related NE frameworks largely relies on their information aggregation mechanism. Nevertheless, such a design leads to low-quality NE on heterophilous networks due to the implicit homophily assumptions. To address this issue, we modify the aggregation mechanism by cutting off connections among aggregation trees and highlighting each node’s local structure.

Specifically, we first define a subnetwork instance of a certain (ego) node v to be its r -ego network $\mathcal{G}_r(v)$. For example, in Figure 3, $\mathcal{G}_2(v)$ represents a 2-ego network instance of \mathcal{G} . We note that given that $\mathcal{G}_r(v)$ captures the local structure of v , it is sufficient to compute a structural representation of v [38].

Anonymisation. However, as shown in Section IV, the rooted aggregation trees of two connected nodes largely overlap which can lead to learning indistinguishable representations for connected nodes. This property is useful in homophilous settings but leads to low quality NE performance on heterophilous networks. To address this, we propose node anonymisation to reduce the overlap of ego networks of connected nodes. Specifically, we anonymise the sampled ego network $\mathcal{G}_r(v)$ by relabelling its nodes to $\{1, 2, \dots, |\mathcal{N}_u^r|\}$, in an arbitrary order, and erasing raw node attributes. Note that node order does not influence the representation quality because most GNNs are invariant to permutations of their inputs [2]. This step ensures that v ’s representation is only influenced by its local structure, as illustrated in Figure 1-(c).

Network structure features. Despite the significant success of GNNs in a variety of network-related tasks, their representation power in network structural representation learning is limited [51]. In order to obtain invariant node structural representations so that nodes with different ego network structures are assigned different representations, we employ the structural features proposed in [24]. In this paper, we adopt variants shortest path distance (SPD) as node structural features ($\tilde{\mathbf{X}}$).

Network structure encoder module. Over the past few years, numerous GNNs have been proposed to learn node representations from network-structured data, including spectral GNNs [9], [23], [50] and spatial GNNs [13], [51]. For the sake of simplicity, we adopt a simple GNN variant, i.e., GCN [22], as the building block of the network structure encoder. The ℓ -th layer of a GCN can be formally defined as:

$$\mathbf{U}^{(\ell)} = \sigma(\widehat{\mathbf{D}}^{-\frac{1}{2}} \widehat{\mathbf{A}} \widehat{\mathbf{D}}^{-\frac{1}{2}} \mathbf{U}^{(\ell-1)} \mathbf{W}^{(\ell)}) \quad (5)$$

with $\widehat{\mathbf{A}} = \mathbf{A} + \mathbf{I}$, where \mathbf{I} is the identity matrix, and $\widehat{\mathbf{D}}$ is the diagonal node degree matrix of $\widehat{\mathbf{A}}$. $\mathbf{U}^{(\ell-1)} \in \mathbb{R}^{n \times d_{\ell-1}}$ is the hidden representation of nodes in layer $\ell - 1$, with $d_{\ell-1}$ being the dimensionality of this layer’s representation, and $\mathbf{W}^{(\ell)} \in \mathbb{R}^{d_{\ell-1} \times d_{\ell}}$ is a trainable parameter matrix. σ is a non-linear activation function such as ReLU or Sigmoid [14] function. Structural representations $\mathbf{U} = \mathbf{U}^{(L)}$ are obtained after successive applications of L layers.

Final node representations. Representations capturing node attributes (\mathbf{H}) and structural context (\mathbf{U}) are combined to obtain expressive and powerful representations as:

$$\mathbf{Z} = \text{COMBINE}(\mathbf{H}, \mathbf{U}) \quad (6)$$

where $\text{COMBINE}(\cdot)$ can be any commonly used aggregation operation in GNNs [51], such as *mean*, *max*, *sum* and *concat*. We utilise *concat* in all our experiments which allows for an independent integration of representations learnt by the dual-channel architecture. In the next subsection, we will introduce the strategy to optimise the entire framework.

C. Non-negative Self-supervised Learning (RC3)

The objective function plays a major role in NE tasks. Several objective functions have been proposed for NE, such as instance network reconstruction loss [21], distribution approximating loss [37] and node distance approximating loss [13]. Nevertheless, none of them is suitable for NE optimisation on heterophilous networks because of the homophily assumptions used to determine (dis)similar pairs. In heterophilous networks, node distance on network alone does not determine (dis)similarity, i.e., connected nodes are not necessarily similar, and nodes far apart are not necessarily dissimilar. This removes the need for connected nodes to be close in the embedding space and for disconnected nodes to be far apart in the embedding space.

Inspired by the latest success of non-negative self-supervised learning (SSL), we adopt the Barlow-Twins [53] as our overall optimisation objective. Overall, Barlow-Twins is a method (originally proposed in the computer vision domain) that learns data representations using a symmetric network architecture and an empirical cross-correlation based loss function. Specifically, it measures the cross-correlation matrix between the output of two identical networks fed with distorted versions of a sample, and makes it as close to the identity matrix as possible. This causes representations of distorted instances of a sample to be similar, increasing the robustness of representations (invariance to small perturbations) and minimising the redundancy between the components of these representations.

Augmentation. As mentioned previously, we propose a dual-channel feature embedding pipeline to adaptively preserve the useful information from raw node attributes and network structure. Therefore, there are two types of model inputs, i.e., node attributes matrix \mathbf{X} and anonymised ego network $\mathcal{G}_r(v)$. Following the widely adopted SSL training strategy [3], [52], we employ two data augmentation methods (f_{aug}), i.e., node attribute masking and edge masking, for distorted instances generation. As shown in Figure 3, with a pair of given masking ratios, i.e., node attribute masking ratio p_x and edge masking ratio p_e , two pairs of distorted instances can be generated:

$$\begin{aligned} f_{aug}^x(\mathbf{X}, p_x) &= (\mathbf{X}^{(1)}, \mathbf{X}^{(2)}) \\ f_{aug}^g(\mathcal{G}_r(v), p_x, p_e) &= (\mathcal{G}_r^{(1)}(v), \mathcal{G}_r^{(2)}(v)) \end{aligned} \quad (7)$$

Barlow-Twins loss function. Two pairs of node representations follow from the pairs of distorted instances, computed with the node attribute encoder and network structure encoder: node attribute representations $\mathbf{H}^{(1)}$ and $\mathbf{H}^{(2)}$, and network structure representations $\mathbf{U}^{(1)}$ and $\mathbf{U}^{(2)}$. We utilise each pair of node representations to compute a cross-correlation matrix

$\mathcal{C} \in \mathbb{R}^{d \times d}$ with d being the dimensionality of input representations. Using node attributes $\mathbf{H}^{(1)}$ and $\mathbf{H}^{(2)}$ as example, results in the following objective function:

$$\mathcal{L}_{BT}(\mathbf{H}^{(1)}, \mathbf{H}^{(2)}) = \sum_i^{|\mathcal{V}|} (1 - C_{ii})^2 + \lambda \sum_i^{|\mathcal{V}|} \sum_{j \neq i}^{|\mathcal{V}|} C_{ij}^2 \quad (8)$$

$$\text{with } C_{ij} = \frac{\sum_b \mathbf{h}_{b,i}^{(1)} \mathbf{h}_{b,j}^{(2)}}{\sqrt{\sum_b (\mathbf{h}_{b,i}^{(1)})^2} \sqrt{\sum_b (\mathbf{h}_{b,j}^{(2)})^2}}$$

where $\lambda > 0$ defines the trade-off between the invariance and redundancy reduction terms, we adopt the default settings as [53]. b is the batch indexes and i, j index the vector dimension of the input representation vectors.

Empowered with Barlow-Twins, we can optimise the framework’s encoders under heterophilous settings. The node attribute encoder is optimised with \mathcal{L}_{BT} (Eq. 8) and \mathcal{L}_{rec} (Eq. 4), and the network structure encoder is optimised with \mathcal{L}_{BT} (Eq. 8). The overall loss function is $\mathcal{L} = \mathcal{L}_{BT}(\mathbf{U}^{(1)}, \mathbf{U}^{(2)}) + \mathcal{L}_{BT}(\mathbf{H}^{(1)}, \mathbf{H}^{(2)}) + \mathcal{L}_{rec}(\mathbf{X}, \hat{\mathbf{X}})$. Final node representations obtained by Eq. 6 contain information from node attributes and structural context, which will be used in downstream tasks.

D. Model Scalability

According to the design for Selene’s framework, we can find that the network structure representation learning module is categorised as a local network algorithm [45], which only involves local exploration of the network structure. On the other hand, the node attribute representation learning module (Autoencoder) naturally support the mini-batch mechanism. Therefore, our design enables Selene to scale to representation learning on large-scale networks and to be friendly to distributed computing settings [38].

VI. EVALUATION

We evaluate our proposed framework, Selene, on benchmark real-world and synthetic datasets and compare with eleven competing methods over node clustering tasks. Note that different from the experimental settings of relevant work [3], [36], [47] which utilise node class labels to train a classifier after obtaining the node representations to predict test nodes, we do not employ any node class label supervision to strictly adhere to the unsupervised learning requirements.

A. Datasets

Real-world datasets. We use a total of 12 real-world datasets (Texas [35], Wisconsin [35], Actor [35], Chameleon [41], USA-Airports [40], Cornell [35], Europe-Airports [40], Brazil-Airports [40], Deezer-Europe [42], Citeseer [22], DBLP [11], Pubmed [22]) in diverse domains (web-page, citation, co-author, flight transport and online user relation). All real-datasets are available online¹. Statistics information are summarised in Table I.

¹<https://pytorch-geometric.readthedocs.io/en/latest/modules/datasets.html>

TABLE I
STATISTICS OF REAL-WORLD DATASETS. $|\mathcal{V}|$: NUMBER OF NODES; $|\mathcal{E}|$: NUMBER OF EDGES; π : DIMENSIONALITY OF NODES FEATURES; OSF: NODES ONLY HAVE STRUCTURE RELATED FEATURES; d_{avg} : AVERAGE DEGREE; $|\mathcal{Y}|$: NUMBER OF POSSIBLE CLASS LABELS; h : HOMOPHILY RATIO;

Dataset	$ \mathcal{V} $	$ \mathcal{E} $	π	OSF	$ \mathcal{Y} $	d_{avg}	h
Texas	183	325	1,703	False	5	1.8	0.108
Wisconsin	251	515	1,703	False	5	2.1	0.196
Actor	7,600	30,019	932	False	5	3.9	0.219
Chameleon	2,277	31,421	2,325	False	5	27.6	0.233
USA-Airports	1,190	13,599	1	True	4	22.9	0.251
Cornell	183	298	1,703	False	5	1.6	0.305
Europe-Airports	399	11,988	1	True	4	30.1	0.309
Brazil-Airports	131	2,077	1	True	4	16.4	0.311
Deezer-Europe	28,281	185,504	31,241	False	2	6.6	0.525
Citeseer	3,327	4,552	3,703	False	6	2.7	0.736
DBLP	4,057	3,528	334	False	4	1.7	0.799
Pubmed	19,717	88,648	500	False	3	4.5	0.802

Synthetic datasets. We generate random synthetic networks with various homophily levels h and node features by adopting a similar approach to [1], [20] but with some modifications. For instance, synthetic networks of [1] have no available contextual node attributes. Specifically, each synthetic network has 10 classes and 500 nodes per class. Nodes are assigned random features sampled from 2D Gaussians (Synthetic- h) or features from real-world dataset [18] (Synthetic-Products- h). Each dataset, i.e., Synthetic and Synthetic-Products, has 10 networks with $h \in [0, 0.1, 0.2, \dots, 0.9]$. Here, we give detailed descriptions of the generation process.

Network generation. We generate synthetic network \mathcal{G} of $|\mathcal{V}|$ nodes with $|\mathcal{Y}|$ different class labels, and \mathcal{G} has $|\mathcal{V}|/|\mathcal{Y}|$ nodes per class. $|\mathcal{V}|$ and $|\mathcal{Y}|$ are two prescribed numbers to determine the size of \mathcal{G} . Synthetic network’s homophily ratio h is mainly controlled by p_{in} and p_{out} , where p_{in} means the possibility of existing an edge between two nodes with the same label and p_{out} is the possibility of existing an edge between two nodes with different labels. Furthermore, the average degree of \mathcal{G} is $d_{avg} = |\mathcal{V}|/|\mathcal{Y}| \cdot \delta$, where $\delta = p_{in} + (|\mathcal{Y}| - 1) \cdot p_{out}$. Following the described network generation process, with given $|\mathcal{V}|$, $|\mathcal{Y}|$ and d_{avg} , we choose p_{in} from $\{0.0001\delta, 0.1\delta, 0.2\delta, \dots, 0.9\delta\}$. Note that the synthetic network generation process requires both p_{in} and p_{out} are positive numbers, hence we use $p_{in} = 0.0001\delta$ to estimate $h = 0$ case.

Node features generation. In order to comprehensively evaluate the performances of different models, we assign each node with statistic features (Synthetic) or real-world contextual node features (Synthetic-Products). For networks with statistic node features, the feature values of nodes are sampled from 2D Gaussian [1]. The mean of Gaussian can be described in polar coordinates: each means has radius 300 and angle $\frac{2\kappa}{10} \times (class\ id)$. For dataset with real-world contextual node features, we first establish a class mapping $\psi: \mathcal{Y} \rightarrow \mathcal{Y}_b$ between classes in the synthetic network \mathcal{Y} to classes of existing benchmark network \mathcal{Y}_b . The only requirement for the target network dataset is that the class size and node set size in the benchmark is larger than that of the synthetic network, i.e., $|\mathcal{Y}_b| \leq |\mathcal{Y}|$ and $|\mathcal{V}| \leq |\mathcal{V}_b|$. In this paper, we adopt the large-scale benchmark, Ognb-Products [18].

TABLE II
 NODE CLUSTERING RESULTS ON HETEROPHILOUS DATASETS. THE BOLD NUMBERS REPRESENT THE TOP-2 RESULTS. OOM: OUT-OF-MEMORY.

Dataset	Metrics	AE	node2vec	struc2vec	LINE	GAE	VGAE	GraphSAGE	SDCN	DGI	GMI	GBT	FAGCN*	Ours	↑ (%)
Texas	ACC	50.49±0.01	48.8±.93	49.73±0.01	49.4±2.08	42.02±1.22	50.27±1.87	56.83±0.56	44.04±0.56	55.74±0.73	35.19±1.2	55.46±0.85	57.92±6.47	64.48±4.35	11.33
	NMI	16.63±0.01	2.58±0.7	18.61±0.01	16.9±1.57	8.49±1.31	11.73±0.95	16.97±1.93	14.24±1.93	8.73±3.63	7.72±0.85	10.17±2.32	23.35±8.95	25.22±8.14	8.01
	ARI	14.6±0.01	-1.62±0.65	20.97±0.01	18.08±1.06	10.83±1.92	21.51±1.81	23.5±2.98	10.65±2.98	8.25±6.82	2.96±0.63	12.1±4.08	22.54±10.88	34.19±11.45	45.49
Wisc.	ACC	58.61±0.26	41.39±0.9	43.03±0.01	39.4±0.59	37.81±0.31	40.0±0.44	46.29±2.44	38.25±2.44	44.58±1.94	36.97±1.15	48.01±4.67	61.91±7.65	71.35±1.55	15.25
	NMI	30.92±0.43	4.23±0.1	11.23±0.01	9.7±1.99	9.19±0.07	9.87±0.48	10.16±0.26	8.46±0.26	10.72±0.81	11.68±1.98	7.55±3.23	27.35±6.57	39.31±2.77	27.13
	ARI	28.53±0.35	-0.48±0.4	11.5±0.01	8.13±0.53	5.2±0.25	7.97±0.35	6.06±0.65	3.67±0.65	10.31±0.72	3.74±1.82	3.85±1.29	31.56±9.39	43.26±3.22	37.07
Actor	ACC	24.19±0.11	25.02±0.04	22.49±0.34	22.7±0.08	23.45±0.04	23.3±0.22	23.08±0.29	24.26±0.1	24.26±0.1	26.18±0.01	24.68±0.48	25.61±0.12	28.22±0.27	10.19
	NMI	0.97±0.03	0.09±0.01	0.04±0.01	0.09±0.01	0.18±0.01	0.21±0.03	0.58±0.14	0.08±0.14	1.38±0.04	0.2±0.0	0.74±0.13	3.22±0.08	4.69±0.69	45.65
	ARI	0.5±0.04	0.06±0.02	-0.05±0.05	0.11±0.01	-0.04±0.01	0.34±0.05	0.22±0.07	-0.01±0.07	0.07±0.03	0.41±0.01	-0.57±0.09	0.34±0.06	1.82±0.05	264.00
Chamel.	ACC	35.68±0.61	21.31±0.26	26.34±1.33	31.97±0.32	32.76±0.01	30.65±0.11	31.04±0.22	33.5±0.22	27.77±0.02	25.73±0.08	32.21±0.85	31.33±0.42	38.49±0.04	7.88
	NMI	10.38±0.46	0.34±0.04	3.55±0.82	10.78±1.0	11.6±0.01	6.86±0.08	10.55±0.07	9.57±0.07	4.42±0.02	2.5±0.09	10.56±1.26	14.71±0.44	20.05±0.12	36.3
	ARI	5.8±0.15	0.02±0.02	1.82±0.42	6.04±0.53	4.4±0.11	4.4±0.11	6.16±0.11	5.86±0.11	1.85±0.01	0.52±0.05	7.01±1.44	5.16±0.46	15.89±0.08	126.68
USA-Air.	ACC	55.24±0.01	26.29±0.03	27.58±0.39	27.17±0.21	30.84±0.25	28.71±1.03	32.96±0.7	33.52±1.0	33.36±0.0	28.69±0.06	34.96±0.01	38.82±0.46	57.39±0.01	3.49
	NMI	30.13±0.01	0.25±0.03	0.44±0.08	0.23±0.04	2.71±0.04	0.55±0.21	2.67±0.37	5.21±1.0	5.52±0.0	0.6±0.01	5.27±0.01	12.3±0.21	29.25±0.01	0.96
	ARI	24.2±0.01	-0.05±0.03	0.09±0.05	-0.08±0.03	2.67±0.07	0.28±0.22	2.52±0.38	1.93±1.0	4.95±0.0	0.29±0.0	3.42±0.01	9.33±0.24	24.69±0.01	2.27
Cornell	ACC	52.19±0.01	50.98±0.01	32.68±0.01	34.1±0.77	43.72±1.25	43.39±0.99	44.7±2.0	36.94±2.0	44.1±2.73	33.55±2.08	52.19±1.68	56.23±8.29	57.81±4.67	2.81
	NMI	17.08±0.01	5.84±0.01	1.54±0.01	2.85±0.21	5.11±0.38	5.46±0.46	4.33±0.93	6.6±0.93	5.79±0.8	5.26±1.33	5.94±1.62	17.08±3.99	17.1±3.45	0.12
	ARI	17.41±0.01	0.18±0.01	-2.2±0.01	-1.54±0.25	6.51±1.74	3.97±0.49	5.64±1.33	3.38±1.33	4.87±2.03	3.05±0.89	0.63±0.23	19.88±13.91	22.85±5.09	14.94
Eu.-Air.	ACC	55.36±1.11	30.78±0.67	36.89±0.9	34.06±0.28	34.84±0.01	34.51±0.67	31.75±1.02	37.37±1.0	35.59±0.32	35.34±0.0	39.75±0.15	42.11±0.0	57.47±0.46	3.81
	NMI	32.44±0.64	3.69±0.19	6.15±1.44	4.77±0.52	10.15±0.01	3.68±0.48	2.1±0.46	8.45±1.0	10.77±0.07	11.08±0.0	9.44±0.01	16.81±0.0	33.74±0.42	4.01
	ARI	24.24±1.3	0.83±0.06	4.49±0.92	2.89±0.61	7.37±0.01	3.02±0.57	1.16±0.41	5.31±1.0	8.44±0.07	8.18±0.0	7.87±0.15	11.98±0.0	25.14±0.47	3.71
Bra.-Air.	ACC	71.68±0.01	30.38±0.31	38.93±0.01	33.74±1.61	36.64±0.01	32.82±1.75	37.02±1.99	38.7±1.0	37.1±0.61	38.93±0.0	40.92±0.53	44.2±0.63	78.77±1.59	9.89
	NMI	49.26±0.01	2.5±0.11	10.23±0.01	2.75±0.94	10.96±0.01	3.7±1.19	6.89±1.47	14.05±1.0	10.64±0.13	12.62±0.08	12.16±0.15	22.67±0.69	55.6±1.18	12.87
	ARI	42.93±0.01	-0.22±0.08	5.45±0.01	0.19±0.77	6.56±0.01	0.6±0.83	4.18±1.59	7.27±1.0	7.02±0.13	9.11±0.03	8.31±0.1	14.4±0.65	52.87±2.46	23.15
Deezer.	ACC	55.88±0.01	52.97±0.02	OOM	52.56±0.06	51.51±0.01	51.27±0.01	51.06±0.01	54.76±0.01	53.16±0.0	OOM	OOM	56.81±0.0	59.75±0.05	5.18
	NMI	0.28±0.01	0.0±0.01	OOM	0.08±0.01	0.13±0.01	0.12±0.01	0.16±0.01	0.17±0.01	0.05±0.0	OOM	OOM	0.27±0.0	0.31±0.02	10.71
	ARI	0.81±0.01	0.02±0.01	OOM	0.23±0.01	0.07±0.01	0.04±0.01	-0.02±0.01	0.61±0.01	-0.23±0.0	OOM	OOM	0.82±0.0	0.89±0.01	8.54

B. Experimental Setup

Competing methods. We compare our framework Selene with 11 competing NE methods. We adopt 3 different shallow competing embeddings methods, including node2vec [12], struc2vec [40] and LINE [44]. We adopt 8 additional deep competing embedding methods, including AE [17], GAE & VGAE [21], GraphSAGE [13], DGI [47], SDCN [5], GMI [36] GBT [3] and FAGCN* [4]. Note that GBT is a self-supervised learning approach that migrates Barlow-Twins approach to network structure data. However, they don't modify the model structure of GNNs but just provide a new model training approach, hence still maintaining a homophily assumption. FAGCN* is a state-of-the-art heterophilous GNN for supervised settings, here we train it with the same mechanism as GBT to adapt it to the unsupervised setting.

Evaluation metrics. We employ three node clustering evaluation metrics: accuracy (ACC), normalised mutual information (NMI) and average rand index (ARI). For each evaluation metric, a significant value means better node clustering performance.

Model implementation. For shallow embedding methods, we set the embedding dimension to 128, the number of random walks of each node to 10 and the walk length to 80. For node2vec, we additionally select p, q over $\{0.25, 0.5, 1, 2\}$ with best clustering performance. We train embedding methods, including AE, GAE, VGAE and SDCN, with the same settings as [5]. Specifically, we train the models end-to-end using all nodes and edges with 30 epochs, and a learning rate of 10^{-3} . For AE, we set the representation dimensions to $\{\pi - 500 - 500 - 200 - 10\}$, where π is the dimensionality of raw node attributes. For GNN-related methods, including GAE, VGAE, GraphSAGE, DGI, GBT, GMI, FAGCN* and Selene, we set their representation dimensions to $\{\pi - 256 - 16\}$. The representation dimensions of SDCN's GCN module are the same as AE. [5] proposes to pretrain the SDCN's AE component to boost its performance, thus we report the best

performance of SDCN with/without pre-trained AE. For DGI, GMI, GBT and Selene, we assign the same GCN [22] encoder and follow the optimisation protocol as [3]. We set $r = 3$ for ego network extraction following [24] and the batch size = 512. For shallow competing methods, we utilise the integrated implementations from GraphEmbedding². For GAE, VGAE, GraphSAGE, DGI and FAGCN* we use the implementation from Pytorch-Geometric³; for AE & SDCN and GMI and GBT, we use the implementation from the published code of SDCN⁴, GMI⁵ and GBT⁶, respectively.

Note that, all experiments are conducted on a single Tesla V100 GPU. For all NN-based methods, we initialise them 10 times with random seeds and select the best solution to follow the similar setting as [5]. After obtaining node representations with each model, we feed the learned representations into a K-means clustering model [15] to get the final clustering prediction. The final clustering section is thus repeated 10 times, and we report the mean/std performance.

C. Experimental Results

Real-world datasets. Node clustering results on homophilous and heterophilous real-world datasets are summarised in Table III and Table II, respectively. In Table II, we see that Selene is the best-performing method in all heterophilous datasets. In particular, compared to the best results of competing models, our framework achieves a significant improvement of up to 15.25% on ACC, 45.65% on NMI and 264% on ARI. Such outstanding performance demonstrates that Selene successfully integrates the important node attributes and network structure information into node representations. An interesting case is the comparison of Selene, FAGCN* and GBT, given

²<https://github.com/shenweichen/GraphEmbedding>

³<https://pytorch-geometric.readthedocs.io/en/latest/>

⁴<https://github.com/bdy9527/SDCN>

⁵<https://github.com/zpeng27/GMI>

⁶<https://github.com/pbielak/graph-barlow-twins>

TABLE III
 NODE CLUSTERING RESULTS ON HOMOPHILOUS DATASETS. THE BOLD NUMBERS REPRESENT THE TOP-2 RESULTS. OOM: OUT-OF-MEMORY.

Dataset	Metrics	AE	node2vec	struc2vec	LINE	GAE	VGAE	GraphSAGE	SDCN	DGI	GMI	GBT	FAGCN*	Ours	↑ (%)
Citeseer	ACC	58.79±0.19	20.76±0.27	21.22±0.45	28.42±0.88	48.37±0.37	55.67±0.13	49.28±1.18	59.86±1.18	58.94±0.43	59.04±0.03	57.21±0.15	47.42±0.27	59.24±2.5	-1.04
	NMI	30.91±0.21	0.35±0.03	1.18±0.08	8.49±0.74	24.59±0.22	32.45±0.1	22.97±0.8	30.37±0.8	32.6±0.38	32.11±0.03	31.9±0.13	20.18±0.26	29.91±2.23	-8.25
	ARI	30.29±0.23	-0.01±0.04	0.17±0.06	3.54±0.56	19.5±0.31	28.34±0.13	19.21±1.33	29.7±1.33	33.16±0.55	33.09±0.04	33.17±0.13	17.93±0.24	29.35±3.1	-11.52
DBLP	ACC	48.5±0.42	29.19±0.06	31.65±0.34	35.34±1.59	57.81±0.02	46.0±0.55	48.68±0.31	61.94±0.31	58.22±0.37	63.28±0.14	73.1±0.37	41.25±1.15	75.14±0.13	2.79
	NMI	18.98±0.35	0.14±0.01	1.33±0.01	3.22±1.28	28.94±0.03	11.57±0.21	16.46±0.33	27.13±0.33	29.98±0.21	33.91±0.07	42.21±0.47	10.6±0.88	43.96±0.14	4.15
	ARI	15.15±0.51	-0.04±0.01	1.39±0.07	2.05±0.44	18.78±0.02	11.68±0.38	13.38±0.26	27.77±0.26	26.81±0.33	28.77±0.13	42.57±0.7	4.32±0.53	46.08±0.29	8.25
Pubmed	ACC	65.34±0.08	39.32±0.07	37.39±0.01	50.53±0.42	42.08±0.03	34.38±0.06	67.66±0.03	61.9±0.03	65.47±0.01	OOM	OOM	56.88±0.11	66.27±0.16	-2.05
	NMI	26.89±0.11	0.02±0.01	0.07±0.01	18.62±2.44	1.28±0.01	0.03±0.01	30.71±0.04	19.71±0.04	28.05±0.02	OOM	OOM	16.91±0.1	28.7±0.03	-6.55
	ARI	25.98±0.14	0.09±0.02	0.06±0.01	8.17±0.17	0.15±0.02	0.0±0.01	29.1±0.05	18.63±0.05	27.25±0.01	OOM	OOM	16.27±0.12	28.21±0.01	-3.06

that FAGCN* and GBT also utilise the Barlow-Twins objective function to optimise a GNN model, and the major difference between FAGCN*, GBT and Selene is the dual-channel features embedding pipeline. Selene has a superior performance in all heterophilous datasets, indicating the necessity to propose an unsupervised heterophilous network embedding model. Simply porting supervised models to unsupervised scenarios is not appropriate. And the dual-channel features embedding pipeline plays a crucial role in improving the representation learning in the heterophily scenario.

Results of node clustering on homophilous networks, contained in Table III, show that Selene achieves competing performance compared to the best-performing methods, consistently performing in the top-2, in all 3 datasets on ACC. This shows Selene’s suitability for homophilous networks and proves the flexibility of the dual-channel feature embedding pipeline.

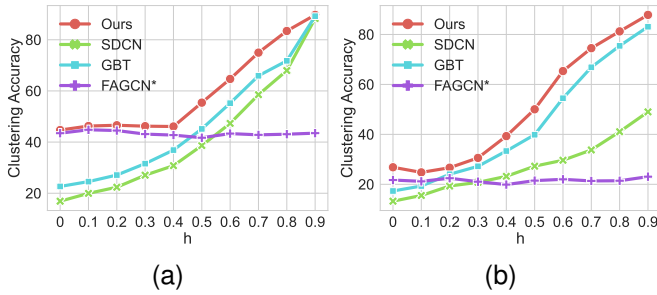


Fig. 4. Clustering accuracy comparison of Selene vs SDCN vs GBT vs FAGCN* on Synthetic (a) and Synthetic-Products (b).

Synthetic networks. We present Selene vs SDCN (state-of-the-art node clustering model) vs GBT (state-of-the-art graph contrastive learning model) vs FAGCN* (state-of-the-art heterophilous GNN model) clustering accuracy in Figure 4. Selene achieves the best performance on the Synthetic dataset and has competitive performance on the Synthetic-Products dataset. This shows that Selene adapts well to homophily/heterophily scenarios with(out) contextually raw node attributes. Moreover, FAGCN* performs worse on 20 synthetic networks, which indicates that the heterophilous GNNs models designed for supervised settings do not adapt well to unsupervised settings because they need supervision information to train the more complex aggregation mechanism.

D. Analysis

Model scalability. Table II and Table III illustrate that two competing methods, i.e., struc2vec, GMI and GBT, have out-of-memory issues on large datasets, i.e., Pubmed and Deezer., an issue which did not arise with Selene. This shows Selene’s advantage in handling large scale networks due to its local network algorithm characteristic. Note that we only use one GPU in experiments, and such an advantage would be more evident in multi-GPU computing scenarios.

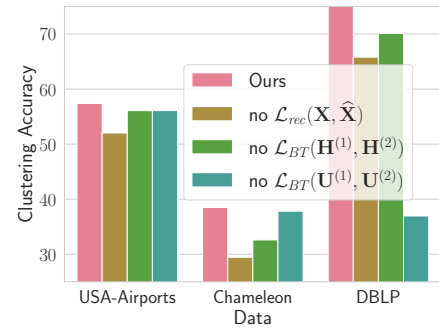


Fig. 5. Loss function exploration. We ablate constituent of our loss function and report Selene’s performance.

Effectiveness of loss function. The objective loss function of Selene contains three components and we thus sought to test the effectiveness of each component. In particular, we ablate each component and evaluate the obtained node representations on two heterophilous datasets (USA-Air, Chamel.) and one homophilous dataset (DBLP). Results shown in Figure 5 indicates that ablation of any component decreases the model’s performance. Specifically, the ablation of $\mathcal{L}_{rec}(\mathbf{X}, \hat{\mathbf{X}})$ causes a steeper performance degradation in heterophilous datasets, and the ablation of $\mathcal{L}_{BT}(\mathbf{U}^{(1)}, \mathbf{U}^{(2)})$ causes a steeper performance degradation in homophilous datasets, which indicates the importance of node attributes and network structure information for heterophilous and homophilous networks, respectively (consistent with observations in Section IV).

Effectiveness of dual-channel feature embedding pipeline. Selene contains a novel dual-channel features embedding pipeline to integrate node attributes and network structure information, thus we conduct an ablation study to explore the effectiveness of this pipeline. We first remove the pipeline and only use the Barlow-Twins loss function to train a vanilla GCN encoding module (such a structure is the same as GBT, hence we remark it as GBT). Next, we add the network

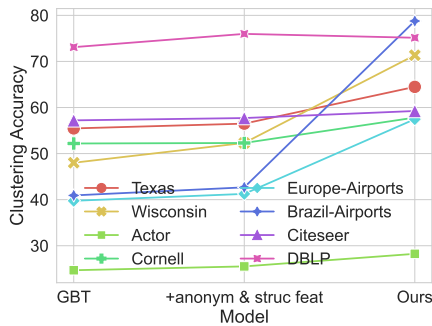


Fig. 6. Framework component exploration. We ablate component of our dual-channel feature embedding pipeline and report Selene’s performance.

structure channel, which includes r -ego network extraction, anonymisation and distortion. Lastly, we add the node attribute channel to form the complete Selene framework. Experimental results are shown in Figure 6. Overall, we observe that the design of each channel is useful for learning better representation, with the node attribute channel playing a major role in the embedding on heterophilous networks. Note that adding the node attribute channel slightly decreases the clustering accuracy for the homophilous dataset, i.e., DBLP, but it is still competitive.

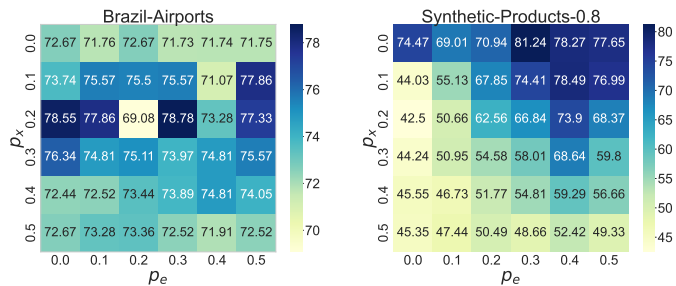


Fig. 7. Hyperparameter influence exploration. We present Selene’s clustering accuracy on two networks with different p_x and p_e .

Influence of p_x and p_e . We present Selene’s clustering accuracy on two networks, i.e., Brazil-Airports ($h = 0.311$) and Synthetic-Products-0.8 with different p_x and p_e in Figure 7. The figure indicates that hyperparameters of augmentation methods have a significant influence on representation quality.

VII. CONCLUSION AND FUTURE DIRECTIONS

In this paper, we focused on the network embedding task with challenging heterophily settings and tackled two main research questions. First, we showed through an empirical investigation that the performance of existing embedding methods that rely on network structure decreases significantly with the decrease of network homophily ratio. Second, to address the identified limitations, we proposed Selene, which effectively fuses node attributes and network structure information without additional supervision. Comprehensive experiments demonstrated the significant performance of Selene, and additional ablation analysis confirms the effectiveness of components of Selene on real-world and synthetic networks. As future work, we propose to explore the *Information*

Bottleneck [46], [48] of network embedding to theoretically define the optimal representation of an arbitrary network and optimally balance expressiveness and robustness against potential external attacks [57].

ACKNOWLEDGMENT

This work is supported by the Luxembourg National Research Fund through grant PRIDE15/10621687/SPsquared. The authors (G.G.) were supported by the ERC-Consolidator Grant No. 724228 (LEMAN).

REFERENCES

- [1] S. Abu-El-Hajja, B. Perozzi, A. Kapoor, N. Alipourfard, K. Lerman, H. Harutyunyan, G. V. Steeg, and A. Galstyan, “Mixhop: Higher-order graph convolutional architectures via sparsified neighborhood mixing,” in *Proceedings of the 2019 International Conference on Machine Learning (ICML)*. JMLR, 2019, pp. 21–29.
- [2] P. W. Battaglia, J. B. Hamrick, V. Bapst, A. Sanchez-Gonzalez, V. F. Zambaldi, M. Malinowski, A. Tacchetti, D. Raposo, A. Santoro, R. Faulkner, Ç. Gülçehre, H. F. Song, A. J. Ballard, J. Gilmer, G. E. Dahl, A. Vaswani, K. R. Allen, C. Nash, V. Langston, C. Dyer, N. Heess, D. Wierstra, P. Kohli, M. Botvinick, O. Vinyals, Y. Li, and R. Pascanu, “Relational inductive biases, deep learning, and graph networks,” *CoRR*, vol. abs/1806.01261, 2018.
- [3] P. Bielak, T. Kajdanowicz, and N. V. Chawla, “Graph barlow twins: A self-supervised representation learning framework for graphs,” *CoRR*, vol. abs/2106.02466, 2021.
- [4] D. Bo, X. Wang, C. Shi, and H. Shen, “Beyond low-frequency information in graph convolutional networks,” in *Proceedings of the 2021 AAAI Conference on Artificial Intelligence (AAAI)*. AAAI, 2021, pp. 3950–3957.
- [5] D. Bo, X. Wang, C. Shi, M. Zhu, E. Lu, and P. Cui, “Structural deep clustering network,” in *Proceedings of the 2020 International Conference on World Wide Web (WWW)*. ACM, 2020, pp. 1400–1410.
- [6] D. Chen, Y. Lin, W. Li, P. Li, J. Zhou, and X. Sun, “Measuring and relieving the over-smoothing problem for graph neural networks from the topological view,” in *Proceedings of the 2020 AAAI Conference on Artificial Intelligence (AAAI)*. AAAI, 2020.
- [7] E. Chien, J. Peng, P. Li, and O. Milenkovic, “Adaptive universal generalized pagerank graph neural network,” in *Proceedings of the 2021 International Conference on Learning Representations (ICLR)*. OpenReview.net, 2021.
- [8] P. Cui, X. Wang, J. Pei, and W. Zhu, “A survey on network embedding,” *IEEE Transactions on Knowledge and Data Engineering*, vol. 31, no. 5, pp. 833–852, 2019.
- [9] M. Defferrard, X. Bresson, and P. Vandergheynst, “Convolutional neural networks on graphs with fast localized spectral filtering,” in *Proceedings of the 2016 Annual Conference on Neural Information Processing Systems (NIPS)*. NIPS, 2016, pp. 3837–3845.
- [10] Y. Dong, Z. Hu, K. Wang, Y. Sun, and J. Tang, “Heterogeneous network representation learning,” in *Proceedings of the 2020 International Joint Conferences on Artificial Intelligence (IJCAI)*. IJCAI, 2020, pp. 4861–4867.
- [11] X. Fu, J. Zhang, Z. Meng, and I. King, “MAGNN: metapath aggregated graph neural network for heterogeneous graph embedding,” in *Proceedings of the 2020 International Conference on World Wide Web (WWW)*. ACM, 2020, pp. 2331–2341.
- [12] A. Grover and J. Leskovec, “node2vec: Scalable feature learning for networks,” in *Proceedings of the 2016 ACM Conference on Knowledge Discovery and Data Mining (KDD)*. ACM, 2016, pp. 855–864.
- [13] W. L. Hamilton, Z. Ying, and J. Leskovec, “Inductive representation learning on large graphs,” in *Proceedings of the 2017 Annual Conference on Neural Information Processing Systems (NIPS)*. NIPS, 2017, pp. 1025–1035.
- [14] J. Han and C. Moraga, “The influence of the sigmoid function parameters on the speed of backpropagation learning,” in *Proceedings of the 1995 International Workshop on Artificial Neural Networks (IWANN)*. Springer, 1995, pp. 195–201.
- [15] J. A. Hartigan and M. A. Wong, “Algorithm as 136: A k-means clustering algorithm,” *Journal of the Royal Statistical Society. Series C (Applied Statistics)*, vol. 28, no. 1, pp. 100–108, 1979.

- [16] K. He, X. Zhang, S. Ren, and J. Sun, "Delving deep into rectifiers: Surpassing human-level performance on imagenet classification," in *Proceedings of the 2015 IEEE International Conference on Computer Vision (ICCV)*. IEEE, 2015, pp. 1026–1034.
- [17] G. E. Hinton and R. R. Salakhutdinov, "Reducing the dimensionality of data with neural networks," *Science*, vol. 313, pp. 504–507, 2006.
- [18] W. Hu, M. Fey, M. Zitnik, Y. Dong, H. Ren, B. Liu, M. Catasta, and J. Leskovec, "Open graph benchmark: Datasets for machine learning on graphs," in *Proceedings of the 2020 Annual Conference on Neural Information Processing Systems (NeurIPS)*. NeurIPS, 2020.
- [19] F. Karimi, M. Génois, C. Wagner, P. Singer, and M. Strohmaier, "Homophily influences ranking of minorities in social networks," *Scientific Reports*, vol. 8, pp. 1–12, 2018.
- [20] D. Kim and A. Oh, "How to find your friendly neighborhood: Graph attention design with self-supervision," in *Proceedings of the 2021 International Conference on Learning Representations (ICLR)*. OpenReview.net, 2021.
- [21] T. N. Kipf and M. Welling, "Variational graph auto-encoders," *CoRR*, vol. abs/1611.07308, 2016.
- [22] —, "Semi-supervised classification with graph convolutional networks," in *Proceedings of the 2017 International Conference on Learning Representations (ICLR)*. OpenReview.net, 2017.
- [23] R. Levie, F. Monti, X. Bresson, and M. M. Bronstein, "Cayleynets: Graph convolutional neural networks with complex rational spectral filters," *IEEE Signal Processing Magazine*, vol. 67, no. 1, pp. 97–109, 2017.
- [24] P. Li, Y. Wang, H. Wang, and J. Leskovec, "Distance encoding - design provably more powerful graph neural networks for structural representation learning," in *Proceedings of the 2020 Annual Conference on Neural Information Processing Systems (NeurIPS)*. NeurIPS, 2020.
- [25] D. Lim, F. Hohne, X. Li, S. L. Huang, V. Gupta, O. Bhalerao, and S. Lim, "Large scale learning on non-homophilous graphs: New benchmarks and strong simple methods," in *Proceedings of the 2021 Annual Conference on Neural Information Processing Systems (NeurIPS)*. NeurIPS, 2021.
- [26] N. Litvak and R. van der Hofstad, "Uncovering disassortativity in large scale-free networks," *Physical review E*, vol. 87, no. 2, p. 022801, 2013.
- [27] A. Makhzani, J. Shlens, N. Jaitly, and I. J. Goodfellow, "Lstm-based encoder-decoder for multi-sensor anomaly detection," *CoRR*, vol. abs/1511.05644, 2015.
- [28] P. Malhotra, A. Ramakrishnan, G. Anand, L. Vig, P. Agarwal, and G. Shroff, "Lstm-based encoder-decoder for multi-sensor anomaly detection," *CoRR*, vol. abs/1607.00148, 2016.
- [29] J. Masci, U. Meier, D. C. Ciresan, and J. Schmidhuber, "Stacked convolutional auto-encoders for hierarchical feature extraction," in *Proceedings of the 2011 International Conference on Artificial Neural Networks (ICANN)*. Springer, 2011, pp. 52–59.
- [30] J. J. McAuley and J. Leskovec, "Learning to discover social circles in ego networks," in *Proceedings of the 2012 Annual Conference on Neural Information Processing Systems (NIPS)*. NIPS, 2012, pp. 548–556.
- [31] T. Mikolov, I. Sutskever, K. Chen, G. S. Corrado, and J. Dean, "Distributed representations of words and phrases and their compositionality," in *Proceedings of the 2013 Annual Conference on Neural Information Processing Systems (NIPS)*. NIPS, 2013, pp. 3111–3119.
- [32] Y. Min, F. Wenkel, and G. Wolf, "Scattering GCN: overcoming over-smoothness in graph convolutional networks," in *Proceedings of the 2020 Annual Conference on Neural Information Processing Systems (NeurIPS)*. NeurIPS, 2020.
- [33] V. Nair and G. E. Hinton, "Rectified linear units improve restricted boltzmann machines," in *Proceedings of the 2010 International Conference on Machine Learning (ICML)*. JMLR, 2010, pp. 807–814.
- [34] A. Y. Ng, M. I. Jordan, and Y. Weiss, "On spectral clustering: Analysis and an algorithm," in *Proceedings of the 2001 Annual Conference on Neural Information Processing Systems (NIPS)*. NIPS, 2001.
- [35] H. Pei, B. Wei, K. C. Chang, Y. Lei, and B. Yang, "Geom-gcn: Geometric graph convolutional networks," in *Proceedings of the 2020 International Conference on Learning Representations (ICLR)*. OpenReview.net, 2020.
- [36] Z. Peng, W. Huang, M. Luo, Q. Zheng, Y. Rong, T. Xu, and J. Huang, "Graph representation learning via graphical mutual information maximization," in *Proceedings of the 2020 International Conference on World Wide Web (WWW)*. ACM, 2020, pp. 259–270.
- [37] B. Perozzi, R. Al-Rfou, and S. Skiena, "Deepwalk: Online learning of social representations," in *Proceedings of the 2014 ACM Conference on Knowledge Discovery and Data Mining (KDD)*. ACM, 2014, pp. 701–710.
- [38] J. Qiu, Q. Chen, Y. Dong, J. Zhang, H. Yang, M. Ding, K. Wang, and J. Tang, "GCC: graph contrastive coding for graph neural network pre-training," in *Proceedings of the 2020 ACM Conference on Knowledge Discovery and Data Mining (KDD)*. ACM, 2020, pp. 1150–1160.
- [39] J. Qiu, Y. Dong, H. Ma, J. Li, K. Wang, and J. Tang, "Network embedding as matrix factorization: Unifying deepwalk, line, pte, and node2vec," in *Proceedings of the 2018 ACM International Conference on Web Search and Data Mining (WSDM)*. ACM, 2018, pp. 459–467.
- [40] L. F. R. Ribeiro, P. H. P. Saverese, and D. R. Figueiredo, "struc2vec: Learning node representations from structural identity," in *Proceedings of the 2017 ACM Conference on Knowledge Discovery and Data Mining (KDD)*. ACM, 2017, pp. 385–394.
- [41] B. Rozemberczki, C. Allen, and R. Sarkar, "Multi-scale attributed node embedding," *Journal of Complex Networks*, vol. 9, no. 2, 2021.
- [42] B. Rozemberczki and R. Sarkar, "Characteristic functions on graphs: Birds of a feather, from statistical descriptors to parametric models," in *Proceedings of the 2020 ACM International Conference on Information and Knowledge Management (CIKM)*. ACM, 2020, pp. 1325–1334.
- [43] J. Tang, M. Qu, and Q. Mei, "Pte: Predictive text embedding through large-scale heterogeneous text networks," in *Proceedings of the 2015 ACM Conference on Knowledge Discovery and Data Mining (KDD)*. ACM, 2015, pp. 1165–1174.
- [44] J. Tang, M. Qu, M. Wang, M. Zhang, J. Yan, and Q. Mei, "Line: Large-scale information network embedding," in *Proceedings of the 2015 International Conference on World Wide Web (WWW)*. ACM, 2015, pp. 1067–1077.
- [45] S. Teng, "Scalable algorithms for data and network analysis," *Foundations and Trends in Theoretical Computer Science*, vol. 12, no. 1-2, pp. 1–274, 2016.
- [46] N. Tishby and N. Zaslavsky, "Deep learning and the information bottleneck principle," in *2015 IEEE Information Theory Workshop (ITW)*. IEEE, 2015, pp. 1–5.
- [47] P. Velickovic, W. Fedus, W. L. Hamilton, P. Liò, Y. Bengio, and R. D. Hjelm, "Deep graph infomax," in *Proceedings of the 2019 International Conference on Learning Representations (ICLR)*. OpenReview.net, 2019.
- [48] T. Wu, H. Ren, P. Li, and J. Leskovec, "Graph information bottleneck," in *Proceedings of the 2020 Annual Conference on Neural Information Processing Systems (NeurIPS)*. NeurIPS, 2020.
- [49] Z. Wu, S. Pan, F. Chen, G. Long, C. Zhang, and P. S. Yu, "A comprehensive survey on graph neural networks," *IEEE Transactions on Neural Networks and Learning Systems*, vol. 32, no. 1, pp. 4–24, 2020.
- [50] B. Xu, H. Shen, Q. Cao, Y. Qiu, and X. Cheng, "Graph wavelet neural network," in *Proceedings of the 2019 International Conference on Learning Representations (ICLR)*. OpenReview.net, 2019.
- [51] K. Xu, W. Hu, J. Leskovec, and S. Jegelka, "How powerful are graph neural networks?" in *Proceedings of the 2019 International Conference on Machine Learning (ICML)*. JMLR, 2019.
- [52] Y. You, T. Chen, Y. Sui, T. Chen, Z. Wang, and Y. Shen, "Graph contrastive learning with augmentations," in *Proceedings of the 2020 Annual Conference on Neural Information Processing Systems (NeurIPS)*. NeurIPS, 2020.
- [53] J. Zbontar, L. Jing, I. Misra, Y. LeCun, and S. Deny, "Barlow twins: Self-supervised learning via redundancy reduction," in *Proceedings of the 2021 International Conference on Machine Learning (ICML)*. JMLR, 2021, pp. 12 310–12 320.
- [54] Z. Zhang, P. Cui, and W. Zhu, "Deep learning on graphs: A survey," *IEEE Transactions on Knowledge and Data Engineering*, 2020.
- [55] J. Zhu, R. A. Rossi, A. B. Rao, T. Mai, N. Lipka, N. K. Ahmed, and D. Koutra, "Graph neural networks with heterophily," in *Proceedings of the 2021 AAAI Conference on Artificial Intelligence (AAAI)*. AAAI, 2021, pp. 11 168–11 176.
- [56] J. Zhu, Y. Yan, L. Zhao, M. Heimann, L. Akoglu, and D. Koutra, "Beyond homophily in graph neural networks: Current limitations and effective designs," in *Proceedings of the 2020 Annual Conference on Neural Information Processing Systems (NeurIPS)*. NeurIPS, 2020.
- [57] D. Zügner, A. Akbarnejad, and S. Günnemann, "Adversarial attacks on neural networks for graph data," in *Proceedings of the 2018 ACM Conference on Knowledge Discovery and Data Mining (KDD)*. ACM, 2018, pp. 2847–2856.